International Journal of Heat and Technology
Vol. 41, No. 3, June, 2023, pp. 694-700
Journal homepage: http://iieta.org/journals/ijht

Thermodynamic and Sealing Performance Analysis of Reciprocating O-Rings in Hydraulic Cylinders

Nana Tao

Institute of Intelligent Manufacturing, Zibo Vocational Institute, Zibo 255000, China

Corresponding Author Email: 10776@zbvc.edu.cn

https://doi.org/10.18280/ijht.410323

Received: 2 February 2023
Accepted: 10 May 2023

Keywords:
O-ring seals, rubber material, Mooney-Rivlin model, finite element analysis, thermodynamics

ABSTRACT

In mechanical engineering practice, the service life and sealing performance of equipment are inextricably linked to the performance of O-ring rubber seals. Moreover, thermodynamic factors play a significant role in the performance of these sealing rings, especially in the high-speed reciprocating motion of hydraulic cylinders. Consequently, an integration of thermodynamic factors into the performance analysis of O-rings is necessary. Using a specific type of O-ring in a hydraulic cylinder as an example, the mechanical properties of the rubber material are characterized through the Mooney-Rivlin model determined by the finite element method and experimental methods, thereby deriving material parameters. Concurrently, an analysis was conducted on how thermodynamic factors like temperature changes, heat conduction, and thermal expansion influence sealing performance. Subsequently, a finite element model of the O-ring seal was established, and a simulation analysis was performed on the mechanical and thermodynamic behaviors of the reciprocating O-ring seal in a hydraulic cylinder under varying temperature and pressure conditions. Lastly, the impact of different compression rates, friction coefficients, and working oil pressures on maximum Von Mises stress and contact stress were investigated, thus providing a theoretical basis for the thermodynamic performance analysis and structural optimization design of O-ring rubber seals.

1. INTRODUCTION

O-ring seals, with their simplistic structure, ease of fabrication, superior sealing performance, easy installation, and minimal dynamic frictional resistance, are extensively applied in hydraulic and pneumatic sealing in mechanical equipment [1]. During the lifting process of hydraulic cylinders, the piston reciprocates frequently, and the O-ring seals therein serve the roles of closure and pressure maintenance. However, the reciprocating motion of the piston generates heat, thereby influencing the sealing performance of the O-rings [2]. Thermodynamic factors such as temperature, thermal conductivity, and the coefficient of thermal expansion could affect the shape, physical properties, and service life of the seals [2, 3].

In hydraulic systems, many outstanding academic achievements exist regarding the static sealing characteristics of seal rings, including research on the groove structure parameters of the seal ring, the failure criteria, deformation analysis under compression, distribution of static contact force, and reliability analysis [4-6]. However, fewer studies have been conducted on the dynamic sealing characteristics of O-rings, especially those that undergo high-speed reciprocating movement.

O-rings are prone to distortion and deformation during assembly, which can even lead to surface abrasions. This can potentially result in equipment seal failure, manifesting as "run, jump, drip, leak" phenomena [7]. However, the physical properties of rubber are influenced by temperature changes. Temperature has a significant impact on the hardness, tensile strength, and elongation at break of rubber [8, 9], which can influence the degree of seal ring deformation during assembly.

The working conditions for high-speed reciprocating O-rings are exceedingly complex. Not only does it include heat exchange between the seal ring and the working medium, but it also involves complex changes in contact pressure. This increases the difficulty of researching its sealing performance [10, 11]. Thermodynamic analysis, such as considering the influence of thermal expansion, thermal conductivity, and thermal stress, could play a pivotal role in understanding this complexity [11, 12].

In this study, the Mooney-Rivlin model has been determined using finite element methods and experimental methods to characterize the mechanical properties of the rubber material, and material parameters have been derived [13]. A finite element model of the O-ring seal has been established, and a simulation analysis of the mechanical behavior of the reciprocating O-ring seal in a hydraulic cylinder has been carried out. Additionally, thermodynamic factors were introduced, considering the influence of different temperatures and thermal conductivities on the maximum Von Mises stress and contact stress. Through research on the thermodynamic properties of hydraulic oil, heat exchange between the seal ring and hydraulic oil, thermal expansion, and thermal stress, this study aims to provide a theoretical basis for the structural optimization design, selection, and failure analysis of O-ring rubber seals [11, 14-16].

2. CONSTITUTIVE MODEL OF RUBBER MATERIALS AND MECHANICAL EXPERIMENTS

2.1 Constitutive model of rubber materials

Rubber, being a common material for O-rings, is recognized as a material with multiple nonlinear characteristics, including material nonlinearity, geometric nonlinearity, and boundary nonlinearity [15]. This renders the analysis and research of rubber exceptionally challenging. Nevertheless, this very complexity has increasingly made rubber an important topic of study at the intersection of solid mechanics, material science, and thermodynamics [17]. In finite element analysis, constitutive theories are typically utilized to describe the hyperelastic behavior of rubber materials. ANSYS incorporates an array of constitutive models, chiefly including the Mooney-Rivlin, Yeoh, and Ogden models. Among these, the Mooney-Rivlin model is the most widely used, capable of simulating the mechanical characteristics of most rubber materials [16].

In 1940, Mooney proposed the large deformation theory of rubber, making two fundamental assumptions about rubber materials used in constitutive models: the first is that rubber is incompressible and isotropic when no deformation occurs; the second is that shear strain follows Hooke's law in a plane perpendicular to a unidirectional tensile or compressive axis [18]. Based on these assumptions, Mooney deduced the following strain energy equation:

$$W = \sum_{ij}^{\infty} C_{ij} (I_1 - 3)^i (I_2 - 3)^j \tag{1}$$

where, W is the strain potential energy; C_{ij} is material parameters related to temperature; I_1 and I_2 are invariants of the Cauchy-Green strain. In practical engineering use, it is difficult to measure all Mooney-Rivlin constants, so a two-parameter model is often adopted, resulting in the Mooney-Rivlin model of rubber, namely:

$$W = C_{10}(I_1 - 3) + C_{01}(I_2 - 3) \tag{2}$$

$$I_1 = \lambda_1^2 + \lambda_2^2 + \lambda_3^2 \tag{3}$$

$$I_2 = \lambda_1^2\lambda_2^2 + \lambda_2^2\lambda_3^2 + \lambda_3^2\lambda_1^2 \tag{4}$$

$$J = \lambda_1^2\lambda_2^2\lambda_3^2 = 1 \tag{5}$$

J is the measure of volume changes caused by deformation. As rubber is an incompressible material, $J = 1$; λ_1, λ_2, and λ_3 are the principal stretches, where the subscripts 1, 2, and 3 refer to three mutually orthogonal directions. In uniaxial stretching, $\lambda_2 = \lambda_3 = 0$, and the principal stretch ratio λ is λ_1, thus:

$$\lambda = \varepsilon + 1 \tag{6}$$

It is important to note that in high-temperature environments, the thermodynamic properties of rubber can have a significant impact on its mechanical behavior. For instance, the thermal expansion coefficient of rubber can influence its volume as temperature changes, thus affecting its physical and mechanical properties [19]. These volume changes can potentially alter the contact surface and hence impact its performance in practical engineering applications. On the other hand, if the temperature changes dramatically, thermal stress may occur, leading to structural changes in the rubber, potentially causing micro-cracks and affecting its long-term performance.

Moreover, the thermal conductivity of rubber can also influence its performance in high-temperature environments. Since rubber is a material with relatively low thermal conductivity, there may be heat accumulation, which will impact its constitutive behavior. In situations that require good heat dissipation, such as in high-speed rotating mechanical equipment, the low thermal conductivity of rubber may lead to excessive temperature, altering its constitutive model and thereby impacting the normal operation of the equipment [20].

2.2 Material testing of rubber

Mechanical experiments on rubber can be categorized into several types, encompassing uniaxial tensile tests, equal biaxial tensile tests, plane tensile tests, compression tests, and shear tests, among others. For the efficient and precise acquisition of data points for the constitutive model of rubber, uniaxial tensile tests are most frequently employed. This is mainly due to their relatively simple execution and ease of implementation. Figure 1 displays a rubber uniaxial tensile dumbbell-shaped standard Type I specimen, as set by the GB/T531.1-2008 standard.

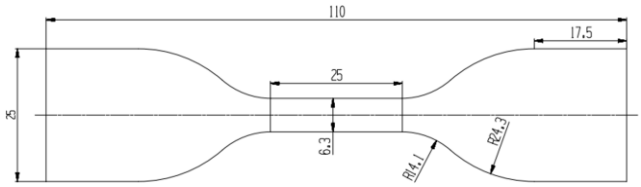

Figure 1. Rubber uniaxial tensile dumbbell-shaped specimen (Type I)

In addition, Figure 2 depicts a rubber tensile testing machine. Utilizing this machine, the clamping force and changes in length of the specimen can be obtained at specified stretching rates. From these measurements, the tensile stress σ and the specimen strain ε can be calculated using formulas (7) and (8).

Figure 2. Rubber tensile testing machine

$$\sigma = \frac{F}{A} \tag{7}$$

In formula (7), F is the tensile force, and A is the minimum cross-sectional area of the dumbbell-shaped specimen.

$$\varepsilon = \frac{\Delta l}{l_0} \tag{8}$$

In formula (8), Δl is the elongation value of the specimen, and l_0 is the initial length of the specimen.

To investigate the mechanical behavior of rubber at different temperatures in greater detail, thermodynamic tests such as Differential Scanning Calorimetry (DSC) and Thermogravimetric Analysis (TGA) can be performed. These tests provide details about the constitutive parameters of rubber under thermodynamic effects, as well as changes in material performance at different temperatures [21].

DSC measures the heat absorbed or released by a material during heating or cooling, aiding in understanding the thermal behavior and phase change processes of rubber. For instance, DSC can be used to determine the glass transition temperature of rubber, an important physical property that indicates the temperature at which rubber transitions from a hard and brittle glassy state to a flexible rubbery state. Moreover, DSC can also measure the melting and crystallization behavior of rubber, as well as its thermal degradation process, providing crucial information for predicting and controlling the performance of rubber in high-temperature environments [22].

On the other hand, TGA can measure changes in a material's mass during heating, aiding in understanding the thermal stability and thermal degradation behavior of rubber. TGA can measure the thermogravimetric loss of rubber at different temperatures, aiding in understanding the thermal degradation temperature and thermal degradation rate of rubber, thus enabling the evaluation of its stability and durability in high-temperature environments. Additionally, TGA can be used to measure the oxidation behavior and fire performance of rubber, providing critical information for the design and optimization of the performance and safety of rubber products [23].

3. FINITE ELEMENT ANALYSIS OF O-RING SEALS

3.1 Parameters of rubber material

The mechanical behavior of rubber materials can be described through the relationship of the Mooney-Rivlin constants C_{10} and C_{01}, as well as the elastic modulus E [18]:

$$\begin{cases} C_{10} + C_{01} = \dfrac{E}{6} \\ C_{01} = \dfrac{C_{10}}{4} \end{cases} \tag{9}$$

Simultaneously, a relationship exists between the elastic modulus E and H_a the Shore hardness as follows:

$$E = \frac{15.75 + 2.15Ha}{100 - Ha} \tag{10}$$

Therefore, by measuring the hardness of O-ring seal samples with H_a Shore durometer, the elastic modulus E and Mooney-Rivlin constants C_{10} and C_{11} can be determined, thereby defining the attributes of the O-ring seal material.

In high-temperature environments, thermodynamic characteristics of rubber significantly influence its mechanical behavior. For instance, thermal expansion can cause a change in the volume of the rubber, while thermal conductivity affects its heat conduction efficiency under heated conditions [24]. Furthermore, thermodynamic tests such as Differential Scanning Calorimetry (DSC) and Thermogravimetric Analysis (TGA) can be carried out to study the mechanical behavior of rubber at varying temperatures. These tests can provide constitution parameters of rubber under thermodynamic effects, as well as information on changes in material properties at different temperatures [21].

3.2 Finite element model

The O-ring seal has an axisymmetric structure. Under normal usage conditions, the seal experiences uniform forces, with equal compression at all positions. Thus, during finite element analysis, the complex three-dimensional model can be simplified to a two-dimensional plane axisymmetric model of the O-ring seal, cylinder, and piston (as shown in Figure 3). The O-ring seal, with dimensions of 10 mm x 1.8 mm, is made of Nitrile Butadiene Rubber (NBR), with a Shore hardness of 85. The width B of the piston's O-ring seal installation slot is 2.4 mm, depth L is 1.2 mm, the chamfer radius of the slot mouth R_1 is 0.3 mm, chamfer radius at the slot bottom R_2 is 0.3 mm, and the installation fillet radius R_3 is 0.5 mm. The piston and cylinder are made of steel, with an elastic modulus of E, Poisson's ratio of 0.3, and density of ρ. The values of C_{10} and C_{01} are calculated to be 0176 and 0.44, respectively, through formulas (9) and (10).

In the finite element model, possible temperature changes that the seal ring may experience should be considered, especially in high-temperature environments where its mechanical properties might alter significantly. For this reason, thermodynamic parameters such as thermal expansion coefficient and thermal conductivity are introduced into the model to simulate these effects [25].

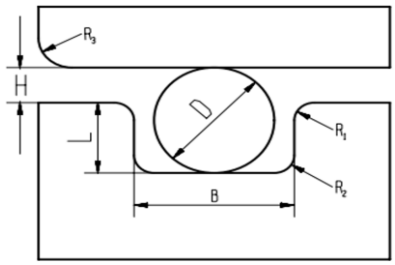

Figure 3. Geometric model of the seal structure

3.3 Contact boundary conditions

During the simulation of dynamic sealing properties of the O-ring seal, contact issues exist between the O-ring seal and the inner wall of the cylinder, as well as the surface of the piston slot. In this model, the Coulomb friction model is used to describe contact friction, with the friction coefficient set to 0.15. Given that the installation of the O-ring seal involves a process of initial stretching followed by compression, the initial compression rate in the model is set to 10%. The cylinder body is fixed, and a displacement of 5 mm is applied to the piston rod in the y direction.

3.4 Load application process

The model load is applied in three steps. Firstly, the pre-compression process of the seal ring is simulated, where the seal ring is tangential to the piston rod on the left and bottom

sides. Secondly, the process of loading the working oil pressure on the seal ring is simulated. Lastly, the reciprocating motion process of the seal ring with the piston is simulated.

During the load application process, thermal expansion or contraction caused by temperature changes should also be considered. Therefore, in the simulation process, while the simulation load is applied, the temperature changes are also simulated to investigate their impact on the performance of the O-ring seal [21].

3.5 Result analysis

Since the O-ring seal is made of rubber, material data obtained from uniaxial tensile tests is inputted into ANSYS software to generate stress-strain curves (as shown in Figure 4). A close match is found between the fitting curve of the Mooney-Rivlin model and the experimental curve, indicating the appropriateness of using the 2-parameter Mooney-Rivlin model to describe the mechanical behavior of Nitrile Butadiene Rubber.

Moreover, by comparing the experimental and simulation results under different temperature conditions, the effect of temperature changes on the mechanical properties of the rubber material can be observed. These results provide a basis for understanding and predicting the performance behavior of O-ring seals in actual applications, especially when subjected to temperature changes [21].

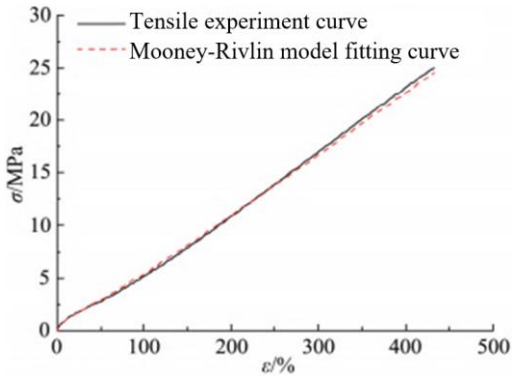

Figure 4. Experimental curve vs. Mooney-Rivlin model fitting curve

4. INFLUENCE OF TYPICAL PARAMETERS ON SEALING PERFORMANCE

4.1 The influence of initial compression ratio

Due to manufacturing errors, an initial radial gap H forms when installing an O-ring, which has a significant effect on the sealing performance. The pre-compression rate is defined with the following formula:

$$\delta = \frac{D-H}{D} \times 100\%$$

In the formula, the cross-sectional diameter D of the O-ring in a free state and the initial radial gap H are denoted. As different initial compression ratios δ of 5%, 10%, 12%, 14%, 15%, 18%, and 20% were tested, the corresponding maximum Von Mises stress and contact stress of the O-ring without pressure were observed as shown in Figure 5. The stress values were found to increase with the initial compression rate, especially when the initial compression rate exceeded 10%. When the initial compression rate exceeded 15%, the difference between the maximum contact stress and the maximum Von Mises stress gradually decreased, suggesting that the O-ring's sealing performance improved, but the potential for damage increased. Therefore, a reasonable design of the initial compression ratio allows for effective control of the stress concentration of the O-ring.

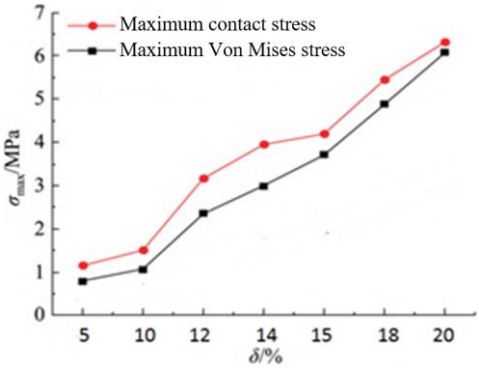

Figure 5. Variation curve of maximum stress of O-ring with different initial compression ratios

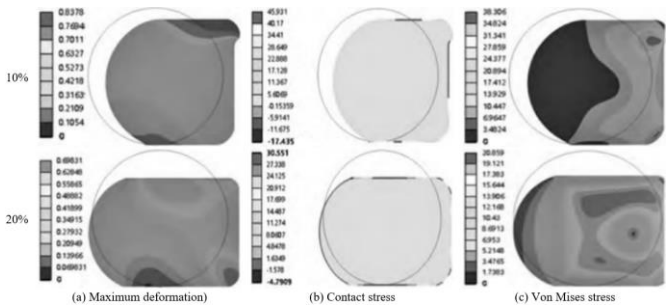

Figure 6. Cloud diagram of maximum deformation, contact stress, and Von Mises stress of dynamic sealing of the O-ring

At 28MPa of working oil pressure, an analysis of the impact of different compression ratios on the sealing performance was conducted, resulting in the O-ring dynamic seal's maximum deformation, contact stress, and Von Mises stress cloud diagram as shown in Figure 6. As the compression rate decreased, the maximum deformation increased as well; the O-ring showed maximum deformation of 0.82 mm and squeezing phenomena at a 10% compression rate. Similarly, the O-ring dynamic seal presented squeezing and stress concentration phenomena at lower compression rates. At a 10% compression rate, the O-ring dynamic seal also showed stress concentration at the site of squeezing, with the maximum Von Mises stress reaching 38MPa, and a high maximum contact stress (45.9MPa) was observed.

4.2 Influence of the friction coefficient

The friction of the contact surface is a major cause of O-ring damage in practical use. Therefore, it is critical to investigate the influence of the friction coefficient (f) on the sealing performance. Given different friction coefficient values (0.05, 0.10, 0.15, 0.20, 0.25, 0.30, 0.35, 0.40) and an initial compression rate of 10%, the maximum Von Mises stress and contact stress curves were obtained as shown in Figure 7. The stress values were found to increase with the friction

coefficient, presenting a sudden change at a friction coefficient of 0.25, highlighting the need for strict control over the contact surface's friction coefficient to avoid stress concentration and extend the lifespan of the O-ring.

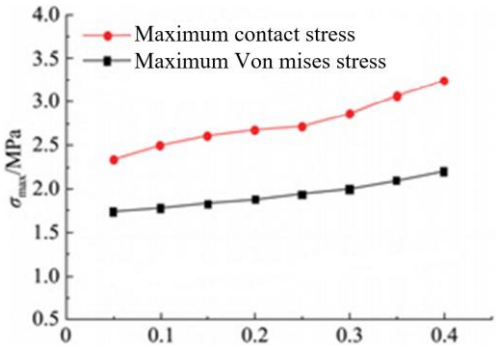

Figure 7. Variation curve of the maximum stress in the O-ring with different friction coefficients

4.3 Influence of working oil pressure

To further explore the impact of working oil pressure on O-ring seals, liquid pressure from 0-28MPa was applied to the same size O-ring static seal at different compression rates. The resulting oil pressure-maximum contact stress curve is shown in Figure 8. Under 10MPa of oil pressure, the maximum contact stress increases linearly with the increase of the O-ring's working oil pressure. When the working oil pressure is higher than 10MPa, the compression rate has a significant impact on the contact stress of the O-ring static seal, with the contact stress of O-ring static seals at lower compression rates appearing to be greater.

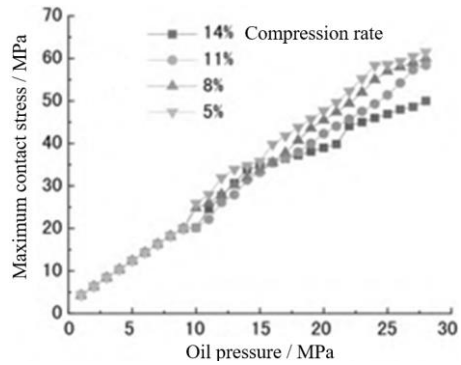

Figure 8. Variation curve of the maximum contact stress with changes in oil pressure

4.4 Influence of temperature

High temperatures have a significant effect on O-rings. Physical properties of rubber materials such as elastic modulus, hardness, thermal expansion coefficient, and weather resistance can change with temperature. These changes may directly or indirectly impact the seal's performance.

4.4.1 Changes in elastic modulus

As temperature increases, the elastic modulus of rubber materials may decrease, implying a reduction in hardness and a less sensitive reaction to stress. This could lead to larger deformations under pressure, affecting sealing performance. Additionally, changes in the elastic modulus could affect the initial compression rate of the seal, altering the contact stress between it and the fittings.

4.4.2 The impact of thermal expansion

As temperature increases, rubber materials undergo thermal expansion. This expansion could result in an increase in the radial or axial dimensions of the seal, altering the gap between it and the fittings, possibly increasing contact stress, and impacting sealing performance. In specific applications, such as high temperature and high pressure environments, thermal expansion could lead to excessive deformation of the seal, preventing it from providing adequate sealing.

4.4.3 The impact of weather resistance

Under high temperatures, the weather resistance of rubber materials can be affected, potentially leading to aging of the seal, reducing its sealing performance. Aging may increase the hardness of the seal, reduce its elasticity, and introduce defects such as cracks, all of which could impact sealing performance.

4.4.4 Experimental analysis

To study the impact of temperature on O-ring performance, a series of experiments were conducted, primarily measuring elastic modulus, determining thermal expansion coefficient, and testing sealing performance. These tests were conducted at different temperatures (e.g., 20℃, 40℃, 60℃, 80℃, 100℃) to gather comprehensive data [25, 26].

(1) Measurement of Elastic Modulus: The elastic modulus of a single O-ring material was measured at different temperatures. Results indicated that with increasing temperature, the elastic modulus typically displayed a decreasing trend, which could be attributed to heightened thermal movement of rubber molecules, thereby reducing elasticity.

(2) Determination of Thermal Expansion Coefficient: By accurately measuring the size changes of an O-ring at different temperatures, the thermal expansion coefficient could be calculated. The results indicated that as temperature increased, radial and axial dimensions of the seal increased, which could impact contact stress between the seal and fittings, thereby affecting sealing performance.

(3) Sealing Performance Testing: The sealing performance of O-rings was tested at different temperatures, with a focus on parameters such as maximum contact stress, maximum deformation, and leak rate. The results showed that as the temperature increased, the maximum contact stress and maximum deformation of the seal increased. Additionally, the leak rate of the seal increased under high temperature conditions, further confirming the impact of temperature on sealing performance.

These experimental results not only help understand the influence of temperature on O-ring performance but also provide a robust basis for.

5. CONCLUSION

(1) Based on the uniaxial tensile experiment, the stress-strain curve of natural rubber material was obtained. By comparing it with the finite element fitting curve, it was discovered that the Mooney-Rivlin model is suitable for describing the material properties of natural rubber.

(2) To ensure the sealing performance of the O-ring, a reasonable pre-compression ratio needs to be selected. Finite element analysis of the O-ring dynamic seal at different

compression ratios under 28 MPa of working oil pressure revealed that a higher O-ring compression rate can prevent squeeze phenomena and avoid stress concentration in high-pressure conditions.

(3) The study of the O-ring static seal suggests that the influence of working oil pressure on the maximum contact stress of the seal ring is approximately linear. Moreover, at higher oil pressure, the maximum contact stress of the O-ring seal with a higher compression ratio is smaller.

(4) Thermodynamic analysis unveiled significant effects of temperature on the performance of O-rings. With rising temperatures, the elastic modulus of the O-ring decreases, the thermal expansion coefficient increases, and the sealing performance may deteriorate. Furthermore, high temperatures can lead to an increase in heat conduction and heat transfer speed, thus affecting the internal stress distribution and wear conditions of the O-ring.

(5) The friction coefficient is closely related to thermodynamics, as the heat generated by friction could potentially elevate the temperature of the O-ring, thereby affecting its performance. When the friction coefficient increases, the maximum contact stress and Von Mises stress of the seal ring also increase, potentially leading to a decrease in sealing performance.

(6) This study not only analyzed the effects of compression ratio, friction coefficient, and working oil pressure on the sealing performance of the O-ring, but also explored the influence of temperature on the O-ring's performance. These involve concepts of thermodynamics, therefore, considering thermodynamic factors in the design and selection of O-rings is of utmost importance. By controlling and optimizing these parameters, the performance and lifespan of O-rings in hydraulic systems can be effectively enhanced.

REFERENCES

[1] Zhao, M., Huang, L., Zhang, Q., Xia, Y., Ping, L. (2020). Study on sealing per - formance and reliability of rubber O-ring by Ansys. China Rubber Industry, 67(2): 131-134. https://doi.org/10.12136/j.issn.1000-890X.2020.02.0131

[2] San Andrés, L., Koo, B. (2019). Effect of lubricant supply pressure on SFD performance: ends sealed with O-rings and piston rings. In Proceedings of the 10th International Conference on Rotor Dynamics–IFToMM, Rio de Janeiro, Brazil, pp. 359-371. https://doi.org/10.1007/978-3-319-99262-4_26

[3] Zhang, J., Hu, Y. (2019). Mechanical behavior and sealing performance of metal sealing system in roller cone bits. Journal of Mechanical Science and Technology, 33: 2855-2862. https://doi.org/10.1007/s12206-019-0533-5

[4] Zhang, D.W., Yang, G.C., Lv, S.C., Tian, C., Li, Z.J. (2023). Fretting behavior of static metal seal and testing apparatus for fretting friction with low/high temperature. Tribology International, 187: 108676. https://doi.org/10.1016/j.triboint.2023.108676

[5] Yu, Y., Cui, Y., Zhang, H., Wang, D., Zhong, J. (2022). A contact model of rough surface for metal static seals considering substrate deformation. Tribology, 43(4): 439-445. https://doi.org/10.16078/j.tribology.2022017

[6] Yuan, T., Li, Z., Li, J., Yuan, Q. (2023). Static and rotordynamic characteristics for supercritical carbon dioxide spiral groove dry gas seal with the tilted seal ring. Journal of Engineering for Gas Turbines and Power, 145(1): 011011. https://doi.org/10.1115/1.4055787

[7] Wang, H., Wang, D., Zhang, H. (2021). Measures and methods to prevent installation damage of O-type sealing ring. Mechanical Engineer, (5): 157-159.

[8] Guo, F., Li, H., Guo, Y., Jia, W., Zhu, Y., Chen, L., Xu, J., Zhang, Y., Wu, J. (2023). Physicochemical properties and reaction characteristics of pyrolysis chars produced from various spent tires components and temperatures: A case study. Fuel, 351: 128798. https://doi.org/10.1016/j.fuel.2023.128798

[9] Konarzewski, M., Stankiewicz, M., Sarzyński, M., Wieczorek, M., Czerwińska, M., Prasuła, P., Panowicz, R. (2023). Properties of rubber-like materials and their blends in wide range of temperatures–experimental and numerical study. Acta Mechanica et Automatica, 17(3): 317-332. https://doi.org/10.2478/ama-2023-0037

[10] Li, Z., Sun, X., Zhang, Y., Hao, M. (2011). Finite element numerical simulation of the sealing performance of O-ring seals. Lubrication Engineering, 36(9): 102-105.

[11] Porter, C., Zaman, B., Pazur, R. (2022). A critical examination of the shelf life of nitrile rubber O-Rings used in aerospace sealing applications. Polymer Degradation and Stability, 206: 110199. https://doi.org/10.1016/j.polymdegradstab.2022.110199

[12] Kong, Y., Shen, M., Zhang, Z., Meng, X., Peng, X. (2019). Thermal characteristics of reciprocating friction of rubber O-Ring against stainless steel surface. Journal of Shanghai Jiaotong University, 53(11): 1352-1358. https://doi.org/10.16183/j.cnki.jsjtu.2019.11.011

[13] Hosseini, S., Rahimi, G. (2023). Experimental and numerical analysis of hyperelastic plates using Mooney-Rivlin strain energy function and meshless collocation method. Engineering Analysis with Boundary Elements, 150: 199-218. https://doi.org/10.1016/j.enganabound.2023.02.024

[14] Zhong, L., Zhao, J.L., Fan, S.W. (2014). Simulation study on O-sealing sealing performance based on ABAQUS software. Coal Mine Machinery, 35(3): 52-54. https://doi.org/10.13436/j.mkjx.201403023

[15] Wang, Z., He, K. (2016). Nonlinear finite element analysis of rubber O-sealing ring. Aerospace Manufacturing Technology, (2): 4-8.

[16] Wang, C., Qin, Y., An, Q. (2013). Finite element analysis for the rubber O ring in a mechanical seal. Journal of East China University of Science and Technology, (6): 761-767.

[17] Wang, Z., Su, M., Duan, X., Yao, X., Han, X., Song, J., Ma, L. (2022). Molecular dynamics simulation of the thermomechanical and tribological properties of graphene-reinforced natural rubber nanocomposites. Polymers, 14(23): 5056. https://doi.org/10.3390/polym14235056

[18] Mooney, M.J. (1940). A theory of large deformation. Journal of Applied Physics, 11(9): 582-592. https://doi.org/10.1063/1.1712836

[19] Martinez, J.S., Toussaint, E., Balandraud, X., Le Cam, J.B., Berghezan, D. (2015). Heat and strain measurements at the crack tip of filled rubber under cyclic loadings using full-field techniques. Mechanics of Materials, 81: 62-71. https://doi.org/10.1016/j.mechmat.2014.09.011

[20] Liu, Y., Chen, W., Jiang, D. (2022). Review on heat generation of rubber composites. Polymers, 15(1): 2.

https://doi.org/10.3390/polym15010002
[21] Alikhani, E., Mohammadi, M., Sabzi, M. (2023). Preparation and study of mechanical and thermal properties of silicone rubber/poly (styrene–ethylene butylene–styrene) triblock copolymer blends. Polymer Bulletin, 80(7): 7991-8012. https://doi.org/10.1007/s00289-022-04440-7
[22] Song, M., Hourston, D.J., Reading, M., Pollock, H.M., Hammiche, A. (1999). Modulated differential scanning calorimetry analysis of interphases in multi-component polymer materials. Journal of Thermal Analysis and Calorimetry, 56: 991-1004. https://doi.org/10.1023/A:1010167920138
[23] He, Z., Song, Y., Wang, J., Xu, W., Guan, H., Pang, Y. (2023). Experimental study on mechanical property degradation of thermal aging laminated rubber bearing. Case Studies in Construction Materials, 18: e02060. https://doi.org/10.1016/j.cscm.2023.e02060
[24] Rodas, C.O., Zaïri, F., Naït-Abdelaziz, M., Charrier, P. (2015). Temperature and filler effects on the relaxed response of filled rubbers: Experimental observations on a carbon-filled SBR and constitutive modeling. International Journal of Solids and Structures, 58: 309-321. https://doi.org/10.1016/j.ijsolstr.2014.11.001
[25] Xu, X., Li, X., Wang, F., Xia, C. (2023). Research on leakage prediction calculation method for dynamic seal ring in underground equipment. Lubricants, 11(4): 181. https://doi.org/10.3390/lubricants11040181
[26] Kömmling, A., Jaunich, M., Goral, M., Wolff, D. (2020). Insights for lifetime predictions of O-ring seals from five-year long-term aging tests. Polymer Degradation and Stability, 179: 109278. https://doi.org/10.1016/j.polymdegradstab.2020.109278